ISSN 0036-0236, Russian Journal of Inorganic Chemistry, 2024, Vol. 69, No. 3, pp. 407–420. © Pleiades Publishing, Ltd., 2024.

PHASE EQUILIBIRA IN INORGANIC SYSTEMS: THERMODYNAMICS AND MODELING

High-Temperature Mass Spectrometric Study of the Vaporization of Oxycarbide MAX Phase Ceramics

V. A. ~~Vorozhtsov~~[a], *, V. L. Stolyarova[a, b], S. I. Lopatin[a, b], and A. L. Shilov[a]

[a] *Grebenshchikov Institute of Silicate Chemistry, Russian Academy of Sciences, St. Petersburg, 199034 Russia*

[b] *St. Petersburg State University, St. Petersburg, 199034 Russia*

**e-mail: v.vorozhcov@rambler.ru*

Received October 11, 2023; revised October 30, 2023; accepted November 2, 2023

Abstract—The vaporization of Ti_2SiC, Ti_3SiC_2, Ti_2AlC, Ti_3AlC_2, Zr_2AlC, and Zr_3AlC_2 ~~carbide~~ MAX ~~phase materials~~ and of oxycarbide systems based on these materials with hafnia additives was examined by Knudsen effusion/mass spectrometry at temperatures up to 2200 K. Atomic aluminum was identified as the major vapor species over the Ti_2AlC, Ti_3AlC_2, Zr_2AlC, and Zr_3AlC_2 samples at 1500 K. The silicon-containing samples were less volatile than the aluminum-containing carbide materials; they ~~volatilized~~ at temperatures above 1900 K to form Si, Si_2, SiC_2, and Si_2C vapor species. The addition of hafnia to the carbides under study led to the formation of oxygen-containing vapor species, particularly Al_2O and SiO, and to a decrease in total vapor pressure over the systems formed. The ~~most difficult to volatile~~ were samples of the Ti_2SiC–HfO_2 oxycarbide system, and among the aluminum-containing oxycarbide systems, samples of the Zr_2AlC–HfO_2 system containing up to 10 mol % and samples of the Ti_2AlC–HfO_2 system with a higher HfO_2 ~~percentage were~~.

Keywords: Knudsen effusion/mass spectrometry, vaporization, carbide MAX phases, vapor pressure

DOI: 10.1134/S0036023623603045

INTRODUCTION

The high-temperature behavior of carbon MAX phase materials and of their oxycarbide systems doped with hafnia has been studied. MAX phases are layered compounds with a hexagonal structure, having the general chemical formula $M_{n+1}AX_n$, where M is a *d* metal, A is a *p* element, X is carbon or nitrogen, and $n = 1$, 2 or 3 [1–3]. In this work, we chose to study vaporization in samples whose chemical composition corresponded to $M_{n+1}AX_n$ MAX phases with M = Ti or Zr, A = Si or Al, X = C, and $n = 1$ or 2.

The MAX phases are known for their unique combination of physical and chemical properties, promising for materials design [1–3]. Carbide MAX phases, for example, retaining the advantages of transition-metal carbides, such as high thermal and electrical conductivity, refractoriness, high elasticity coefficients and low thermal expansion coefficients [2], are distinguished by enhanced crack resistance and resistance to oxidation and corrosion [4–6]. Therefore, MAX phases can be used as high-temperature ceramics or additives to enhance the stability of highly refractory materials based on zirconium/hafnium borides in oxygen-containing environments at temperatures above 2273 K [5]. The electrochemical, thermal, and catalytic properties of MAX phases are notable, facilitating the development of, respectively, ohmic contacts, heat exchangers, and oxidation and hydrogenation catalysts on their basis [3]. The MAX phases are precursors for other promising nanomaterials, namely maxenes [5, 6]. Due to their resistance to oxidation, corrosion, and ionizing radiation, MAX phases are of particular interest for use in the nuclear industry [3, 4], e.g., as materials for the cladding of fuel elements of nuclear reactors [7–9]. The carbide MAX phase material Zr_2AlC and an oxycarbide system containing zirconium oxide and Zr_2AlC, have shown high resistance in a prototype corium melt at temperatures up to K, thereby opening up wide opportunities for their application as elements of the core of nuclear reactors [10]. Additives of thermally strong oxides to carbon phases can further increase the refractory properties and oxidation resistance of the materials [11], which makes it relevant to study oxycarbide MAX phase systems.

As mentioned above, however, many MAX phase materials are prepared or perform at high temperatures, which can lead to selective vaporization of their most volatile components and, as a consequence, to an uncontrolled change in their physical and chemical properties. Thus, for the successful use of carbide MAX phases and oxycarbide MAX phase systems, it is necessary, as a first stage, to study their stability at high temperatures in order to identify their temperature limits of thermal stability and the products that will volatilize under heating.

There is information in the literature on an experimental study of the vaporization of individual carbides, summarized in Kazenas and Tsvetkov's monograph [12]. Individual aluminum carbide, when vaporized from graphite effusion cells, turns into vapor in the form of atomic aluminum while the condensed phase becomes enriched in carbon [13]:

$$Al_4C_3(cr) = 4Al(gas) + 3C(cr). \quad (1)$$

Hereafter, the physical state of the substance in chemical equations is indicated in parentheses: "(cr)" stands for a solid, and "(gas) for a gas.

The vapor pressure of atomic aluminum over the $Al_4C_3 + C$ system in the temperature range 1321–1607 K is described by the equation

$$\log p(Al, Pa) = -\frac{18000}{T} + 11.74, \quad (2)$$

where $p(i)$ is the partial vapor pressure of the ith molecular vapor species and T is absolute temperature.

According to Drowart et al. [14], the vapor over individual silicon carbide during when it is vaporized from a graphite effusion cell consists of atomic silicon Si, its dimer Si_2, and silicon carbides SiC_2 and Si_2C:

$$SiC(cr) = Si(gas) + C(cr). \quad (3)$$

The temperature-dependent partial vapor pressure for Si, Si_2, SiC_2, and Si_2C molecular vapor species over silicon carbide in the range 2149–2316 K is described by the following equations, respectively:

$$\log p(Si, Pa) = -\frac{29339 \pm 157}{T} + (13.98 \pm 0.07), \quad (4)$$

$$\log p(Si_2, Pa) = -\frac{37783 \pm 1667}{T} + (15.16 \pm 0.75), \quad (5)$$

$$\log p(SiC_2, Pa) = -\frac{35561 \pm 2063}{T} + (15.84 \pm 0.93), \quad (6)$$

$$\log p(Si_2C, Pa) = -\frac{35395 \pm 1641}{T} + (15.64 \pm 0.74). \quad (7)$$

In the Ti–C system, a TiC_x solid solution was identified, referred to as the δ phase. The highest amount of carbon in the δ phase TiC_x depends on temperature and does not exceed 49.2 mol %. At a higher carbon percentage, δ-TiC_x + C two-phase equilibrium occurs over a wide temperature: 300–2800 K [15]. TiC_x vaporizes incongruently [16, 17] with selective volatilization of titanium as atomic titanium. In addition, the vapor above the TiC_x vaporized from tungsten or tantalum Knudsen cells features the following molecular species (in the decreasing order of partial pressures): C_3, C, C_2, TiC_2, C_5, C_4, and TiC_4 [16, 18]. The temperature-dependent partial pressure of atomic titanium over the TiC_x–C system in the range 2518–2790 K is described by the following equation [18]:

$$\log p(Ti, Pa) = -\frac{28950}{T} + (11.28 \pm 0.74). \quad (8)$$

However, information on the vaporization of carbide MAX phases and oxycarbide MAX phase systems has not been found in the literature. Therefore, the purpose of this work was a mass-spectrometric study of the vaporization of carbide MAX phase materials of composition Ti_2AlC, Ti_3AlC_2, Zr_2AlC, Zr_3AlC_2, Ti_2SiC, and Ti_3SiC_2, and (for the first time) of oxycarbide systems based on the specified samples with additives of hafnia, which is one of the most thermally stable oxides. We should mention the following. Firstly, the Ti_2AlC, Ti_3AlC_2, Zr_2AlC, Zr_3AlC_2, Ti_2SiC, and Ti_3SiC_2 are used here to denote the as-batch chemical compositions of samples, without taking into account the actual phase composition of the material. For example, the notation "Ti_2SiC" indicates that the amounts of reagents during the synthesis of the sample were selected in such a way as to ensure the ratio of mole fractions of elements as Ti : Si : C = 2 : 1 : 1, but it does not imply that the synthesis would yield an individual MAX phase Ti_2SiC, which is not thermodynamically stable and has not yet been synthesized [19, 20]. The identified as-synthesized phase compositions of samples will appear below in the section "Experimental". Secondly, aluminum carbide is the most volatile of the individual carbides discussed above. Therefore, those who study the high-temperature behavior of aluminum-containing carbide and oxycarbide systems should expect selective vaporization of aluminum to occur at temperatures below 1600 K.

EXPERIMENTAL

A total of six samples of MAX phase carbide materials (Ti_2AlC, Ti_3AlC_2, Zr_2AlC, Zr_3AlC_2, Ti_2SiC, and Ti_3SiC_2) and 18 samples of oxycarbide systems containing 10, 50, and 80 mol % HfO_2 were prepared (Table 1). The samples were synthesized using high-temperature sintering in a vacuum oven and by hot pressing from various precursor materials at various temperatures. The details of the syntheses of carbide MAX phase materials and oxycarbide MAX phase systems are described elsewhere [21–26]. The highest synthesis temperatures were 1773 and 2073 K. The chemical and phase compositions of the synthesized samples were studied by energy-dispersive X-ray spectral microanalysis and X-ray powder diffraction. The Crystallographica Search Match software suite and the JCPDS file were used to identify compounds in X-ray powder diffraction patterns. The phase compositions were quantified in the Crystallographica Search Match software suite by the least squares analysis of the difference between the calculated (theoretical) and measured profiles and intensities of X-ray diffraction peaks. The results of phase analysis of samples synthesized at 1773 and 2073 K appear in Table 2.

Table 1. Elemental compositions of carbide and oxycarbide MAX phase materials synthesized in this work, as probed by energy-dispersive X-ray spectral analysis

Sample No.	As-batch composition, mol %	As-analyzed amounts of elements, at %						
		Ti	Si	C	Al	Zr	Hf	O
1	Ti_2SiC	42.6	21.8	35.6	–	–	–	–
2	Ti_3SiC_2	50.5	11.8	37.7	–	–	–	–
3	Ti_2AlC	54.5	–	27.8	17.8	–	–	–
4	Ti_3AlC_2	45.7	–	39.9	14.3	–	–	–
5	Zr_2AlC	–	–	66.2	11.9	21.9	–	–
6	Zr_3AlC_2	–	–	39.5	28.4	32.1	–	–
7	$90Ti_2SiC–10HfO_2$	35.6	18.1	23.5	–	–	2.1	20.7
8	$50Ti_2SiC–50HfO_2$	24.7	11.7	19.1	–	–	14.5	30.0
9	$20Ti_2SiC–80HfO_2$	17.0	–	16.4	–	–	30.8	36.8
10	$90Ti_3SiC_2–10HfO2$	36.2	11.2	36.5	–	–	1.2	14.9
11	$50Ti_3SiC_2–50HfO_2$	31.1	7.6	27.9	–	–	10.5	22.8
12	$20Ti_3SiC_2–80HfO_2$	19.1	–	20.3	–	–	26.1	34.5
13	$90Ti_2AlC–10HfO_2$	31.4	–	14.0	13.6	–	2.4	38.6
14	$50Ti_2AlC–50HfO_2$	23.1	–	18.0	12.6	–	13.8	32.5
15	$20Ti_2AlC–80HfO_2$	14.3	–	12.2	8.8	–	25.6	39.2
16	$90Ti_3AlC_2–10HfO_2$	39.7	–	20.8	13.6	–	1.6	24.3
17	$50Ti_3AlC_2–50HfO_2$	25.7	–	36.3	8.1	–	10.0	19.9
18	$20Ti_3AlC_2–80HfO_2$	17.0	–	14.0	7.4	–	24.4	37.2
19	$90Zr_2AlC–10HfO_2$	–	–	45.6	10.8	20.5	2.7	20.4
20	$50Zr_2AlC–50HfO_2$	–	–	20.4	10.5	22.2	14.6	32.2
21	$20Zr_2AlC–80HfO_2$	–	–	20.7	6.6	12.4	25.4	34.9
22	$90Zr_3AlC_2–10HfO_2$	–	–	14.4	16.4	16.2	11.0	42.0
23	$50Zr_3AlC_2–50HfO_2$	–	–	25.5	15.8	14.3	1.9	42.5
24	$20Zr_3AlC_2–80HfO_2$	–	–	20.6	9.9	10.1	23.3	36.0

The increasing synthesis temperature brings about a change in phase composition of the product, in particular, an increase in the percentage of MAX phases and the preferential formation of binary oxides and carbides, such as Al_2O_3, HfO_2, $HfTi_2O$, and SiC, TiC, ZrC, and HfC. Therefore, it was proposed to compare the vapor composition over MAX phase–HfO_2 samples synthesized at different temperatures, in order to identify the sensitivity of vaporization to the phase composition of the sample.

The investigation tool used was Knudsen effusion/mass spectrometry [27, 28] on an MS-1301 mass spectrometer. Samples were vaporized from graphite twin Knudsen cells. The diameters of the effusion holes in both compartments of the effusion cell were 0.6 mm; the diameters of the evaporation areas were 6 mm. Thus, the design of the effusion cells ensured the conditions of dynamic equilibrium between the condensed phase and vapor inside each compartment of the cell. The effusion cells were placed in a metal casing made of molybdenum sheet, as electron bombardment was used to heat the cells. The other parameters of the equipment used did not differ from standard ones and were described previously [29, 30]. The effusion cell temperature was measured on an EOP-66 optical pyrometer. The molecular beam effluent from the Knudsen cell was ionized in an ion source by slow electrons with energy of 30 eV to obtain a mass spectrum of the vapor over the test sample.

The partial pressures of molecular vapor species over the samples were determined by comparing ion currents [27, 28]:

$$p(i) = p(s)\frac{I(i^+)T(i)\sigma(s)\gamma(s^+)f(s^+)}{I(s^+)T(s)\sigma(i)\gamma(i^+)f(i^+)}, \quad (9)$$

Table 2. Phase compositions of carbide and oxycarbide MAX phase materials synthesized in this work at maximum temperatures of 1773 and 2073 K, as probed by X-ray powder diffraction

Sample No.	As-batch composition, mol %	$T = 1773$ K		$T = 2073$ K	
		phase	amount, mol %	phase	amount, mol %
1	Ti_2SiC	Ti_3SiC_2 TiC	33.83 66.17	Ti_3SiC_2 TiC	3.03 96.97
2	Ti_3SiC_2	Ti_3SiC_2 TiC	29.40 70.60	Ti_3SiC_2 TiC	1.55 98.45
3	Ti_2AlC	Ti_2AlC TiC	40.11 59.89	Ti_2AlC TiC	4.86 95.14
4	Ti_3AlC_2	Ti_3AlC_2 TiC	21.37 78.63	Ti_3AlC_2 TiC	4.19 95.81
5	Zr_2AlC	Zr_2AlC ZrC	18.52 81.48	Zr_2AlC ZrC	7.41 92.59
6	Zr_3AlC_2	Zr_3AlC_2 ZrC	12.90 87.10	Zr_3AlC_2 ZrC	4.06 95.94
7	$90Ti_2SiC–10HfO_2$	Ti_3SiC_2 TiC TiO_x HfO_2 $HfSiO_4$	7.85 29.98 29.87 21.53 10.76	SiC TiC	10.78 89.22
8	$50Ti_2SiC–50HfO_2$	Ti_3SiC_2 TiC TiO_x HfO_2	7.60 13.09 13.99 65.33	SiC TiC $HfTi_2O$	10.81 70.65 18.54
9	$20Ti_2SiC–80HfO_2$	TiC HfO_2	13.93 86.07	TiC $HfTi_2O$	9.28 90.72
10	$90Ti_3SiC_2–10HfO_2$	Ti_3SiC_2 TiC TiO_x SiC HfO_2	1.43 26.39 49.87 11.46 10.84	SiC TiC	10.45 89.55
11	$50Ti_3SiC_2–50HfO_2$	Ti_3SiC_2 TiC TiO_x HfO_2	6.62 10.92 26.43 56.03	SiC TiC HfO_2 $HfO_{2\ cubic}$	4.97 35.38 27.07 32.58
12	$20Ti_3SiC_2–80HfO_2$	TiC TiO_x HfO_2 $HfO_{2\ cubic}$	10.88 18.32 48.32 22.49	TiC HfO_2 $HfO_{2\ cubic}$	41.63 18.10 40.28
13	$90Ti_2AlC–10HfO_2$	Ti_2AlC TiC TiO_x HfO_2 Al_2O_3	19.64 39.30 13.86 20.01 7.18	TiC HfO_2 Al_2O_3	68.43 26.56 5.01

Table 2. (Contd.)

Sample No.	As-batch composition, mol %	$T = 1773$ K		$T = 2073$ K	
		phase	amount, mol %	phase	amount, mol %
14	$50Ti_2AlC–50HfO_2$	Ti_2AlC TiC TiO_x HfO_2 Al_2O_3	10.69 8.50 23.24 52.41 5.16	TiC HfO_2 $HfO_{2\ cubic}$ Al_2O_3	42.44 25.00 23.47 9.09
15	$20Ti_2AlC–80HfO_2$	Ti_2AlC TiC TiO_x HfO_2 Al_2O_3	2.19 9.26 6.08 76.99 5.48	TiC HfO_2 $HfO_{2\ cubic}$ Al_2O_3	10.74 45.17 38.11 5.99
16	$90Ti_3AlC_2–10HfO_2$	Ti_3AlC_2 TiC TiO_x HfO_2 Al_2O_3	6.29 60.77 19.51 7.79 5.64	TiC $HfO_{2\ cubic}$ Al_2O_3	58.01 15.51 26.48
17	$50Ti_3AlC_2–50HfO_2$	Ti_3AlC_2 TiC TiO_x HfO_2 Al_2O_3	6.38 6.97 38.52 42.85 5.27	TiC HfO_2 $HfO_{2\ cubic}$ Al_2O_3	35.67 30.34 28.22 5.77
18	$20Ti_3AlC_2–80HfO_2$	Ti_3AlC_2 TiC TiO_x HfO_2 Al_2O_3	1.77 7.34 7.74 80.95 2.20	TiC HfO_2 $HfO_{2\ cubic}$ Al_2O_3	32.90 51.13 9.87 6.10
19	$90Zr_2AlC–10HfO_2$	Zr_2AlC ZrC HfO_2 Al_2O_3	9.92 66.25 12.27 11.56	ZrC HfC	75.69 24.31
20	$50Zr_2AlC–50HfO_2$	Zr_2AlC ZrC HfC HfO_2 $HfO_{2\ cubic}$ Al_2O_3	10.35 6.91 27.60 21.92 19.22 14.00	ZrC HfC HfO_2 $HfO_{2\ cubic}$ Al_2O_3	76.11 7.68 5.91 8.16 2.15
21	$20Zr_2AlC–80HfO_2$	ZrC HfC HfO_2 $HfO_{2\ cubic}$ Al_2O_3	6.20 13.58 57.86 20.06 2.31	ZrC HfC HfO_2 $HfO_{2\ cubic}$ Al_2O_3	23.64 15.44 13.72 35.11 12.09
22	$90Zr_3AlC_2–10HfO_2$	Zr_3AlC_2 ZrC HfO_2 Al_2O_3	9.02 33.30 42.01 15.67	ZrC HfC	79.74 20.26

Table 2. (Contd.)

Sample No.	As-batch composition, mol %	$T = 1773$ K		$T = 2073$ K	
		phase	amount, mol %	phase	amount, mol %
23	$50Zr_3AlC_2$–$50HfO_2$	Zr_3AlC_2 HfC HfO_2 $HfO_{2\ cubic}$ Al_2O_3	10.81 41.02 41.79 2.10 4.28	ZrC HfC $HfO_{2\ cubic}$ Al_2O_3	54.13 39.25 4.23 2.40
24	$20Zr_3AlC_2$–$80HfO_2$	ZrC HfC HfO_2 $HfO_{2\ cubic}$ Al_2O_3	7.30 17.55 60.56 11.24 3.34	ZrC HfC HfO_2 $HfO_{2\ cubic}$ Al_2O_3	11.23 44.56 28.03 13.63 2.55

where the *i* and *s* refer to the test sample and the pressure reference, respectively; $\sigma(i)$ is the optimization cross section of the *i*th molecular species; $\gamma(i^+)$ is the conversion factor of the secondary electron multiplier; and $f(i^+)$ is the isotopic distribution of the i+th ion in the mass spectrum of the vapor obtained by ionization of the *i*th molecular species.

To study vaporization, the test sample was placed in one compartment of the effusion cell, and the pressure reference was placed in the reference compartment of the cell. When carbide MAX phase samples were studied, individual aluminum carbide or silicon carbide was used as pressure references, for which the temperature-dependent partial pressures of molecular vapor species were previously determined. For oxycarbide MAX phase–HfO_2 systems, the pressure references used were respective carbide samples: Ti_2AlC, Ti_3AlC_2, Zr_2AlC, Zr_3AlC_2, Ti_2SiC, and Ti_3SiC_2, the partial vapor pressures of molecular vapor species over which were determined in this work. Gold is, as a rule, used as a reference in the determination of partial pressures of molecular vapor species by the comparison of ion currents; the International Union of Pure and Applied Chemistry recommended the temperature dependence of Au partial vapor pressure over gold [31]. However, gold is known to form strongly bonded compounds with carbon [12]. Its reactivity decreases as a result, causing date distortion. It was for this reason that we chose individual carbides to be pressure references. In addition, partial vapor pressures over test samples were measured during vaporization from graphite cells under the settings where reaction with carbon at high temperatures could occur, which could shift the composition of the condensed phase. For this reason, in order to gain correct Knudsen effusion/mass spectrometry data, it was necessary to provide identical vaporization conditions for test carbide phases and for individual carbides; in this work, we accomplished this by simultaneously evaporating samples from different compartments of the same graphite effusion cell in one experiment. Alternate measurements of ion current intensities in the vapor mass spectra over the test sample and over the individual carbide made it possible to identify quantitative differences in the nature of vaporization between carbide MAX phase materials and Al_4C_3 or SiC.

The atomic aluminum partial pressures over aluminum-containing carbide MAX phase materials were determined by modified Eq. (9):

$$p(\mathrm{Al}) = p_s(\mathrm{Al})\frac{I(\mathrm{Al}^+)}{I_s(\mathrm{Al}^+)}, \qquad (10)$$

where the Al partial vapor pressure over individual carbide Al_4C_3 (p_s(Al)) was found by Eq. (2).

A relationship similar to Eq. (10) was used to determine Si partial vapor pressures over silicon-containing samples. The partial vapor pressures of Si_2, SiC_2, and Si_2C molecular vapor species over the studied MAX phase materials were determined by the following relationship:

$$p(i) = p_s(\mathrm{Si})\frac{I(i^+)T(i)\sigma_s(\mathrm{Si})\gamma_s(\mathrm{Si}^+)f_s(\mathrm{Si}^+)}{I_s(\mathrm{Si}^+)T_s(\mathrm{Si})\sigma(i)\gamma(i^+)f(i^+)}, \qquad (11)$$

where $i = Si_2$, SiC_2, or Si_2C; the conversion factor of the secondary electron multiplier $\gamma(i^+)$ is taken to be proportional to the molecular weight of the ion: $1/\sqrt{M(i^+)}$; the ionization cross sections for atoms were taken from [32]; the Si_2 ionization cross section was calculated using the Mayer and Lynch relationship [33]; and the ionization cross sections of SiC_2 and Si_2C molecules were found by the additivity rule [28].

RESULTS AND DISCUSSION

Vaporization of Carbide MAX Phase Materials

In the vapor mass spectra over aluminum carbide Al_4C_3 and over aluminum-containing carbide materi-

als Ti_2AlC, Ti_3AlC_2, Zr_2AlC, and Zr_3AlC_2, Al^+ ions with an appearance energy of 6.0 eV were identified starting at ca. 1500 K. Comparison to the ionization energy of atomic aluminum [34] showed that those ions appeared in the mass spectrum as a result of direct ionization of the Al vapor species. The Ti^+ and C_3^+ ions appeared in the vapor mass spectra over test samples at far higher temperatures (1870 and 2300 K, respectively). This indicates that selective vaporization of atomic aluminum occurred when samples of aluminum-containing carbide materials were heated up to 1500 K in vacuo (under a residual gas pressure of about 10^{-3} Pa), and carbon, as well as titanium or zirconium, accumulated in the condensed phase.

Ion current intensity measurements in vapor mass spectra over the studied carbide MAX phase materials served to determine the temperature-dependent partial pressures of atomic aluminum over samples **3**–**6** (Table 1), whose compositions were Ti_2AlC, Ti_3AlC_2, Zr_2AlC, and Zr_3AlC_2, respectively, in the temperature range 1500–1700 K:

$$\log p(\mathrm{Al,Pa}) = -\frac{25038 \pm 505}{T} + 15.68 \pm 0.32, \quad (12)$$

$$\log p(\mathrm{Al,Pa}) = -\frac{26483 \pm 934}{T} + 17.09 \pm 0.59, \quad (13)$$

$$\log p(\mathrm{Al,Pa}) = -\frac{26120 \pm 14529}{T} + 15.83 \pm 0.90, \quad (14)$$

$$\log p(\mathrm{Al,Pa}) = -\frac{29234 \pm 857}{T} + 18.16 \pm 0.54. \quad (15)$$

The temperature-dependent partial vapor pressures over Ti_2AlC, Ti_3AlC_2, Zr_2AlC, and Zr_3AlC_2 carbide MAX phase materials are presented in Fig. 1 and in Tables S1–S4 in the attachment. Ti_2AlC has the highest thermal stability in the Al_4C_3, Ti_2AlC, and Ti_3AlC_2 series. The atomic aluminum partial vapor pressures over Al_4C_3 and Ti_3AlC_2 match each other within the determination error, but the goodness of match worsens as temperature rises. The Zr_3AlC_2 sample is less volatile than titanium-containing phases are, although above 1550 K, the Al partial vapor pressures over Ti_2AlC and Zr_3AlC_2 become undistinguishable within the experimental error. Zr_2AlC is the least volatile of the tested aluminum-containing carbides. Thus, the volatilities of the studied carbide MAX phase materials increase in the following order: $Zr_2AlC < Zr_3AlC_2 < Ti_2AlC < Ti_3AlC_2$.

In vapor mass spectra over SiC, Ti_2SiC, and Ti_3SiC_2 samples, the Si^+, Si_2^+, SiC_2^+, and Si_2C^+ were identified starting at 1900 K. Some difficulties arose from the overlap of ions in the vapor mass spectrum over the studied samples with the signals from the ionization of residual gases of the vacuum system. A reliable quantitative measurement of Si^+ ion current intensity at a mass-to-charge ratio of 28 (for the most abundant silicon isotope) failed because of the high ion current intensities from nitrogen N^{2+} and carbon monoxide CO^+. Therefore, measurements of Si^+ ion current intensities could only be carried out at a mass-to-charge ratio of 30, for a silicon isotope with a molecular weight of 30, the amount of which was 3.12%. The SiC^+ ion with a molecular weight of 40 overlaps with a high Ar^+ background signal at the appropriate mass-to-charge ratio. Due to the low SiC percentage in the vapor over silicon carbide [14], it is not possible to measure the SiC^+ ion current at mass-to-charge ratios of 41 and 42. It should be mentioned here that an MS-1301 mass spectrometer has an electrical shutter and a mechanical shutter designed to separate the "useful" ionic current intensities associated with the test sample from the background signal. However, they shut off not only the Si^+ and SiC^+ ion currents, but also part of the $N_2^+ + CO^+$ and Ar^+ background signals, which interfered with the quantitative results.

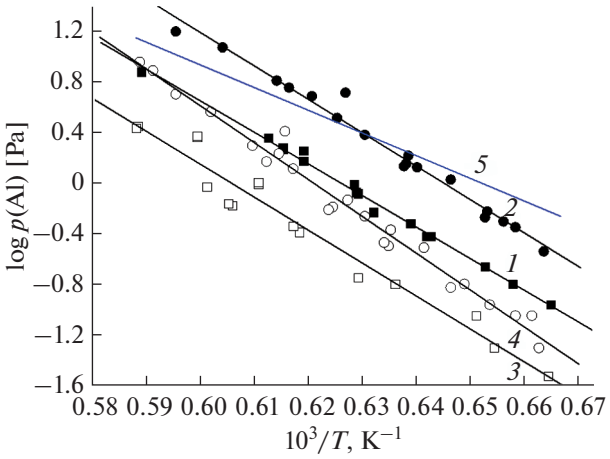

Fig. 1. Temperature-dependent Al partial vapor pressure over carbide materials containing (*1*) Ti_2AlC, (*2*) Ti_3AlC_2, (*3*) Zr_2AlC and (*4*) Zr_3AlC_2, as determined by Knudsen effusion/mass spectrometry in this work, against the respective data for (*5*) Al_4C_3 according to Eq. (2) [13].

The above-listed ions (Si^+, Si_2^+, SiC_2^+, and Si_2C^+) identified in vapor mass spectra over SiC, Ti_2SiC, and Ti_3SiC_2 =carbide samples are all molecular ions [14]. The Ti^+ and C_3^+ ions were detected in vapor mass spectra over samples **1** and **2**, whose as-batch compositions were Ti_2SiC and Ti_3SiC_2, respectively (Table 1), at 2330 K. The data obtained imply that the vapor over the studied silicon-containing carbide materials consists of a mixture of atomic silicon, Si_2, SiC_2, and Si_2C.

Comparative measurements of temperature-dependent ion current intensities from Si^+, Si_2^+, SiC_2^+, and Si_2C^+ ions gave the temperature-dependent partial pressures of Si, Si_2, SiC_2, and Si_2C vapor molecu-

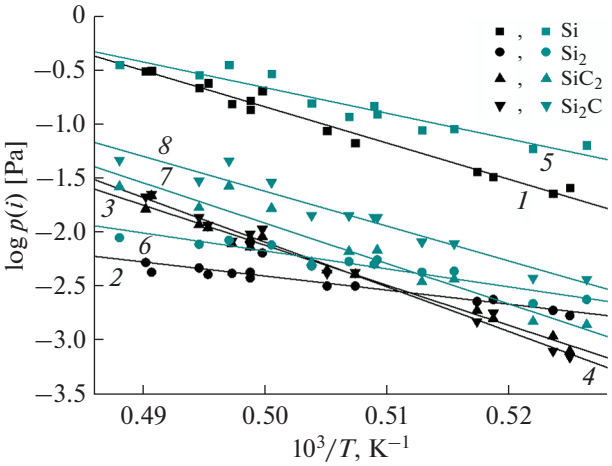

Fig. 2. Temperature-dependent partial vapor pressures of (*1*, *5*) Si, (*2*, *6*) Si_2, (*3*, *7*) SiC_2, and (*4*, *8*) Si_2C over samples **1** and **2** (Table 1) of composition (*1*–*4*) Ti_2SiC and (*5*–*8*) Ti_3SiC_2 according to Eqs. (16)–(23), determined by Knudsen effusion/mass spectrometry in this work.

lar species over sample **1** (Eqs. (16)–(19)) and sample **2** (Table 1; Eqs. (20)–(23)) in the range 1900–2050 K:

$$\log p(\mathrm{Si,Pa}) = -\frac{33677 \pm 1528}{T} + (16.01 \pm 0.77), \quad (16)$$

$$\log p(\mathrm{Si_2,Pa}) = -\frac{13095 \pm 1626}{T} + (4.14 \pm 0.82), \quad (17)$$

$$\log p(\mathrm{SiC_2,Pa}) = -\frac{37240 \pm 1297}{T} + (16.50 \pm 0.65), \quad (18)$$

$$\log p(\mathrm{Si_2C,Pa}) = -\frac{41500 \pm 1600}{T} + (18.66 \pm 0.81), \quad (19)$$

$$\log p(\mathrm{Si,Pa}) = -\frac{23852 \pm 2417}{T} + (11.27 \pm 1.23), \quad (20)$$

$$\log p(\mathrm{Si_2,\ Pa}) = -\frac{16688 \pm 1817}{T} + (6.17 \pm 0.92), \quad (21)$$

$$\log p(\mathrm{SiC_2,Pa}) = -\frac{37539 \pm 3536}{T} + (16.86 \pm 1.79), \quad (22)$$

$$\log p(\mathrm{Si_2C,Pa}) = -\frac{32428 \pm 2543}{T} + (14.60 \pm 1.30). \quad (23)$$

The thus-calculated partial vapors of molecular vapor species over samples **1** and **2** (Ti_2SiC and Ti_3SiC_2, respectively) are shown in Fig. 2 and in Tables S5 and S6; their values indicate that Ti_2SiC has the least total vapor pressure in the SiC, Ti_2SiC, and Ti_3SiC_2 series. Therefore, Ti_2SiC is the most difficult-to-volatile carbide material of those studied in this work.

Vaporization of Oxycarbide MAX Phase–HfO_2 Systems

When the vaporization of MAX phase–HfO_2 systems was studied, a sample of the oxycarbide system being studied was vaporized from one compartment of the twin effusion cell, and the carbide MAX phase material was evaporated from the comparison compartment, as mentioned in the Section "Experimental".

Preliminary experiments showed that carbide MAX phase materials are far more volatile than oxycarbide samples are. Therefore, it was impossible to conduct experiments by the differential mass spectrometric method where the cell compartments with the test sample and pressure reference would be alternately moved onto the optical axis of the mass spectrometer without changing the temperature. On the one hand, at low temperatures (~1500 K), at which aluminum-containing carbide MAX phase materials vaporize, the ion current intensities in vapor mass spectra over oxycarbide samples, as a rule, are at the sensitivity threshold of the mass spectrometer. On the other hand, there are two factors limiting the measurements for the sample and reference at high temperatures, at which the vapor mass spectra over oxycarbide systems are recorded reliably. Firstly, the atomic aluminum partial pressure over a carbide MAX phase material under the specified conditions significantly exceeds the upper limit of pressure measurements by the Knudsen method (13 Pa). Secondly, at high temperatures, the selective vaporization of aluminum from the carbide sample changes the composition of the condensed phase, which does not allow the experimentally obtained values to be attributed to the initial composition of the material. Therefore, in this work, we first measured the Al^+ ion current intensity in the vapor mass spectrum over a carbide MAX phase material at the temperature at which the oxycarbide sample did not vaporize. Then, the evaporator with the effusion cell was moved to the position to measure the ion current intensities in the vapor mass spectrum over the MAX phase–HfO_2 system, and the cell temperature was increased in order to measure the temperature-dependent ion current intensities in the vapor mass spectrum over the test oxycarbide sample. To determine the partial pressures of molecular vapor species over the MAX phase–HfO_2 system, the Al^+ ion current intensity in the vapor mass spectrum over the carbide sample was recalculated using Eqs. (12)–(15) to refer it to the temperature at which the Al^+ intensity in vapor mass spectra over the oxycarbide sample was measured.

It should be especially noted that numerous ions generated by the ionization of highly volatile organic substances, CO, and CO_2 were identified in the vapor mass spectrum during the initial heating of the effusion cells with test samples. For this reason, the vacuum system of the mass spectrometer did not cope with pumping off residual gases to a high vacuum, so after each incremental increase in temperature we had to wait for some time for the vacuum to be restored to

a value that would keep the device's protective system from triggering.

In vapor mass spectra over aluminum-containing MAX phase–HfO_2 systems, Al^+ and Al_2O^+ ions with an appearance energy of 6.0 and 7.7 eV, respectively, were identified starting at 1500 K. Comparison to the ionization energies of Al and Al_2O vapor species [34] showed that the identified ions were direct ionization products. Noteworthy, the vapor mass spectra over aluminum-containing carbide MAX phase materials also featured an Al^+ ion, and not Al_2O^+. The atomic aluminum partial pressures over MAX phase–HfO_2 oxycarbide systems were determined by Eq. (10), where the Al partial vapor pressure over aluminum-containing carbide samples (p_s(Al)) was determined by Eqs. (12)–(15). The Al_2O partial pressures over the studied oxycarbide systems were determined by the relationship below, which is an analogue of Eq. (11):

$$p(Al_2O) = p_s(Al)\frac{I(Al_2O^+)\sigma_s(Al)\gamma_s(Al^+)}{I_s(Al^+)\sigma(Al_2O)\gamma(Al_2O^+)}, \quad (24)$$

where the aluminum ionization cross sections were taken from [32], and Al_2O ionization cross sections were calculated as for a dialuminum oxide molecule. The dialuminum ionization cross section is 1.8 × σ(Al) [28], and the dialuminum oxide ionization cross section can be calculated as 0.65 × $\sigma(Al_2)$ = 1.17. The calculated values appear in Table S7; they were used to estimate the slopes of temperature-dependent partial pressures of molecular vapor species over the studied oxycarbide samples.

In the Ti_2AlC–HfO_2 system, temperature-dependent Al and Al_2O partial vapor pressures were determined over the following samples:

— 90 mol % Ti_2AlC–10 mol % HfO_2 in the temperature range 1600–1795 K:

$$\log p(Al, Pa) = -\frac{23715 \pm 988}{T} + 14.52 \pm 0.36, \quad (25)$$

$$\log p(Al_2O, Pa) = -\frac{25675 \pm 790}{T} + 15.28 \pm 0.32, \quad (26)$$

— 50 mol % Ti_2AlC–50 mol % HfO_2 in the temperature range 1627–1821 K:

$$\log p(Al, Pa) = -\frac{32906 \pm 2480}{T} + 18.17 \pm 1.435, \cos^{-1}\theta, \quad (27)$$

$$\log p(Al_2O, Pa) = -\frac{30168 \pm 2419}{T} + 16.00 \pm 1.38, \quad (28)$$

— 20 mol % Ti_2AlC–80 mol % HfO_2 in the temperature range 1632–1821 K:

$$\log p(Al, Pa) = -\frac{24380 \pm 1330}{T} + 12.79 \pm 0.43, \quad (29)$$

$$\log p(Al_2O, Pa) = -\frac{25084 \pm 806}{T} + 12.85 \pm 0.47. \quad (30)$$

The total Al and Al_2O vapor pressure over Ti_2AlC–HfO_2 oxycarbide samples is far lower than the Al partial vapor pressure over sample **3** (Ti_2AlC according to Table 1). The partial vapor pressure of the Al molecular vapor species over the Ti_2AlC–HfO_2 system decreases as the HfO_2 percentage increases. The Al_2O fraction in the total vapor pressure increases, as temperature rises, over the 90 mol % Ti_2AlC–10 mol % HfO_2 and 20 mol % Ti_2AlC–80 mol % HfO_2 samples, and decreases over the 50 mol % Ti_2AlC–50 mol % HfO_2 sample.

In the Ti_3AlC_2–HfO_2 system, temperature-dependent Al and Al_2O partial vapor pressures were determined over the following samples:

— 90 mol % Ti_3AlC_2–10 mol % HfO_2 in the temperature range 1501–1615 K:

$$\log p(Al, Pa) = -\frac{27109 \pm 1767}{T} + (17.00 \pm 1.14), \quad (31)$$

$$\log p(Al_2O, Pa) = -\frac{29897 \pm 1907}{T} + (18.40 \pm 1.23), \quad (32)$$

— 50 mol % Ti_3AlC_2–50 mol % HfO_2 in the temperature range 1699–1815 K:

$$\log p(Al, Pa) = -\frac{28595 \pm 654}{T} + 15.94 \pm 0.37, \quad (33)$$

$$\log p(Al_2O, Pa) = -\frac{24576 \pm 1257}{T} + 13.05 \pm 0.72, \quad (34)$$

— 20 mol % Ti_3AlC_2–80 mol % HfO_2 in the temperature range 1729–1835 K:

$$\log p(Al, Pa) = -\frac{24238 \pm 2281}{T} + 13.19 \pm 1.28, \quad (35)$$

$$\log p(Al_2O, Pa) = -\frac{27658 \pm 1160}{T} + 14.63 \pm 0.65. \quad (36)$$

The total Al and Al_2O vapor pressure over Ti_3AlC_2–HfO_2 oxycarbide samples is far lower than the Al partial vapor pressure over sample **4** (Ti_3AlC_2 according to Table 1). The Al_2O fraction in the total vapor pressure increases, as temperature rises, over the 90 mol % Ti_3AlC_2–10 mol % HfO_2 and 20 mol % Ti_3AlC_2–80 mol % HfO_2 and decreases the 50 mol % Ti_3AlC_2–50 mol % HfO_2 sample. The Ti_3AlC_2–HfO_2 system has a higher volatility compared to that of the Ti_2AlC–HfO_2 system.

In the Zr_2AlC–HfO_2 system, temperature-dependent Al and Al_2O partial vapor pressures were determined over the following samples:

— 90 mol % Zr_2AlC–10 mol % HfO_2 in the temperature range 1685–1777 K:

$$\log p(\mathrm{Al,Pa}) = -\frac{28535 \pm 1229}{T} + 16.63 \pm 0.71, \quad (37)$$

$$\log p(\mathrm{Al_2O,Pa}) = -\frac{32198 \pm 1410}{T} + 18.01 \pm 0.81, \quad (38)$$

— 50 mol % Zr_2AlC–50 mol % HfO_2 in the temperature range 1699–1824 K:

$$\log p(\mathrm{Al,Pa}) = -\frac{27154 \pm 1492}{T} + 15.05 \pm 0.84, \quad (39)$$

$$\log p(\mathrm{Al_2O,Pa}) = -\frac{19387 \pm 1482}{T} + 9.96 \pm 0.84, \quad (40)$$

— 20 mol % Zr_2AlC–80 mol % HfO_2 in the temperature range 1725–1844 K:

$$\log p(\mathrm{Al,Pa}) = -\frac{27136 \pm 641}{T} + 14.72 \pm 0.36, \quad (41)$$

$$\log p(\mathrm{Al_2O,Pa}) = -\frac{29249 \pm 1029}{T} + 15.40 \pm 0.58. \quad (42)$$

The total Al and Al_2O vapor pressure over Zr_2AlC–HfO_2 oxycarbide samples is far lower than the Al partial vapor pressure over sample **5** (Zr_2AlC according to Table 1). The Al_2O fraction in the total vapor pressure increases, as temperature rises, over the 90 mol % Zr_2AlC–10 mol % HfO_2 and 20 mol % Zr_2AlC–80 mol % HfO_2 samples and decreases over the 50 mol % Zr_2AlC–50 mol % HfO_2 sample.

In the Zr_3AlC_2–HfO_2 system, temperature-dependent Al and Al_2O partial vapor pressures were determined over the following samples:

— 90 mol % Zr_3AlC_2–10 mol % HfO_2 in the temperature range 1634–1765 K:

$$\log p(\mathrm{Al,Pa}) = -\frac{27438 \pm 1293}{T} + 16.84 \pm 0.76, \quad (43)$$

$$\log p(\mathrm{Al_2O,Pa}) = -\frac{30297 \pm 2121}{T} + 18.05 \pm 1.24, \quad (44)$$

— 50 mol % Zr_3AlC_2–50 mol % HfO_2 in the temperature range 1687–1785 K:

$$\log p(\mathrm{Al,Pa}) = -\frac{25995 \pm 1217}{T} + 15.95 \pm 0.70, \quad (45)$$

$$\log p(\mathrm{Al_2O,Pa}) = -\frac{31377 \pm 2413}{T} + 18.67 \pm 1.38. \quad (46)$$

— 20 mol % Zr_3AlC_2–80 mol % HfO_2 in the temperature range 1699–1805 K:

$$\log p(\mathrm{Al,Pa}) = -\frac{26223 \pm 1287}{T} + 15.64 \pm 0.83, \quad (47)$$

$$\log p(\mathrm{Al_2O,Pa}) = -\frac{31152 \pm 1881}{T} + 18.07 \pm 1.07. \quad (48)$$

The total Al and Al_2O vapor pressure over Zr_3AlC_2–HfO_2 oxycarbide samples is far lower than the Al partial vapor pressure over sample **6** (Zr_3AlC_2 in Table 1). The Al_2O fraction in the total vapor pressure increases, as temperature rises, over all studied Zr_3AlC_2–HfO_2 samples. The Zr_3AlC_2–HfO_2 system has a higher volatility compared to that of the Zr_2AlC–HfO_2 system.

In the vapor mass spectra over Ti_2SiC–HfO_2 and Ti_3SiC_2–HfO_2 oxycarbide systems, Si^+, SiC^+, SiO^+, Si_2^+, SiC_2^+, and Si_2C^+ ions were identified starting at ca. 1950 K. The determination of the molecular precursors of these ions showed that they are all products of direct ionization. We should mention that the Si^+, SiC^+, and SiO^+ ions are superimposed on the N_2^+ + CO^+, Ar^+, and CO_2^+ background signals. For this reason, the Si^+, SiC^+, and SiO^+ ion current intensities were measured at the temperature at which useful signals (shut off by the electrical shutter of the mass spectrometer) with mass-to-charge ratios of 28, 40, and 44 were in excess over the background signals. At a mass-to-charge ratio of 44, for example, in addition to a high background signal from the CO_2^+ ion, there is an ion current shut off by the electrical shutter that largely corresponds to the SiO^+ ion. The appearance energy of this ion is 10.6 eV, which corresponds to the ionization energy of silicon monoxide [34], while the ionization energy of CO_2 is 13.8 eV [34]. Thus, the vapor over Ti_2SiC–HfO_2 and Ti_3SiC_2–HfO_2 systems in the temperature range 1950–2100 K consists of Si, SiO, SiC, SiC_2, Si_2, and Si_2C.

The determination of temperature-dependent Si^+, SiO^+, and SiC^+ ion current intensities is difficult due to the fact that the electrical and mechanical shutters of the mass spectrometer both shut off not only the Si^+, SiC^+, and SiO^+ ions of the vapor mass spectrum over the studied samples, but also part of the N_2^+ + CO^+, Ar^+, and CO_2^+ background signals. Therefore, the investigation of vaporization of the Ti_2SiC–HfO_2 and Ti_3SiC_2–HfO_2 systems was further reduced to the determination of the temperature-dependent partial vapor pressures of the SiC_2 and Si_2C molecular vapor species. The Si_2^+ ion current intensity was at the sensitivity threshold of the mass spectrometer and, accordingly, was not measured quantitatively.

In the Ti_2SiC–HfO_2 system, the temperature-dependent partial vapor pressures of SiC_2 and Si_2C were determined over the 90 mol % Ti_2SiC–10 mol % HfO_2 sample in the temperature range 1995–2115 K, the 50 mol % Ti_2SiC–50 mol % HfO_2 sample in the

Table 3. Factors in the equation for the temperature-dependent decimal logarithm of SiC_2 and Si_2C partial vapor pressures over samples of $Ti_{n+1}SiC_n$–HfO_2 (n = 1 or 2) oxycarbide systems, determined by Knudsen effusion/mass spectrometry in this work

HfO_2, mol %	Temperature range, K	$\log p(i)$ [Pa] = $-A/T + B$			
		SiC_2		Si_2C	
		A	*B*	*A*	*B*
The Ti_2SiC–HfO_2 system					
0	1900–2050	37240 ± 1297	16.50 ± 0.65	41500 ± 1600	18.66 ± 0.81
10	1995–2115	39294 ± 746	17.24 ± 0.36	41789 ± 1000	18.52 ± 0.29
50	2004–2115	41552 ± 949	18.37 ± 0.44	36620 ± 1220	15.90 ± 0.61
80	2051–2135	38954 ± 1211	16.84 ± 0.64	35118 ± 850	15.02 ± 0.41
The T_3SiC_2–HfO_2 system					
0	1900–2050	37539 ± 3536	16.86 ± 1.79	32428 ± 2543	14.60 ± 1.30
10	2016–2112	39294 ± 1195	17.24 ± 0.54	41789 ± 1620	18.52 ± 0.78
50	1995–2124	41369 ± 1214	18.44 ± 0.40	38971 ± 1430	17.58 ± 0.59
80	2011–2104	41018 ± 1214	17.98 ± 0.40	37575 ± 1430	16.60 ± 0.59

temperature range 2004–2115 K, and the 20 mol % Ti_2SiC–80 mol % HfO_2 sample in the temperature range 2051–2135 K. The factors of equations for those temperature-dependent partial vapor pressures of molecular vapor species over Ti_2SiC–HfO_2 samples are listed in Table 3.

The SiC_2 and Si_2C partial vapor pressures over Ti_2SiC–HfO_2 oxycarbide samples were far lower than over sample **1** (Ti_2SiC in Table 1).

In the Ti_3SiC_2–HfO_2 system, the temperature-dependent partial vapor pressures of SiC_2 and Si_2C were determined over the 90 mol % Ti_3SiC_2–10 mol % HfO_2 sample in the temperature range 2016–2112 K, the 50 mol % Ti_3SiC_2–50 mol % HfO_2 sample in the temperature range 1995–2124 K, and the 20 mol % Ti_3SiC_2–80 mol % HfO_2 sample in the temperature range 2011–2104 K (Table 3).

The SiC_2 and Si_2C partial vapor pressures over Ti_3SiC_2–HfO_2 oxycarbide samples were far lower than over sample **2** (Ti_3SiC_2 in Table 1). The total of the SiC_2 and Si_2C partial vapor pressures over the Ti_3SiC_2–HfO_2 oxycarbide samples is several times the respective value over the Ti_2SiC–HfO_2 samples containing equal hafnia percentages. We may conclude that the Ti_3SiC_2–HfO_2 system has a higher volatility than that of the Ti_2SiC–HfO_2 system.

Altogether, the Knudsen effusion/mass spectrometric study of Ti_2AlC, Ti_3AlC_2, Zr_2AlC, Zr_3AlC_2, Ti_2SiC, and Ti_3SiC_2 carbide MAX phase materials and their reaction products with hafnia implies that the samples containing titanium, silicon, and silicon and stable up to 1900 K and have the least volatility. Of the SiC, Ti_2SiC, and Ti_3SiC_2 carbide materials, sample **1** (Ti_2SiC in Table 1) has the least volatility. Hafnia additives decrease the partial vapor pressures of the Si_2C and SiC_2 molecular vapor species over the Ti_2SiC–HfO_2 system.

The increasing order of Al partial vapor pressures for aluminum-containing carbide MAX phase materials is $Zr_2AlC < Zr_3AlC_2 < Ti_2AlC < Ti_3AlC_2$.

Sample **5** of as-batch composition Zr_2AlC has the least volatility in the range of temperatures studied. When doped with hafnia, the carbide systems have their volatility order changing. Sample **19**, which also contains the Zr_2AlC phase, has the lowest sum of Al and AlO partial vapor pressures among the carbide systems containing 10 mol% HfO_2. The total vapor pressures over the 90 mol % Ti_2AlC–10 mol % HfO_2 and 90 mol % Zr_3AlC_2–10 mol % HfO_2 samples match each other within the determination error (Fig. 3). The thus-derived increasing order of volatilities is as follows: 90 mol % Zr_2AlC–10 mol % HfO_2 < 90 mol % Ti_2AlC–10 mol % HfO_2 ~ 90 mol % Zr_3AlC_2–10 mol % HfO_2 ≪ 90 mol % Ti_3AlC_2–10 mol % HfO_2.

In the 50 mol % HfO_2 systems, the least sum of Al and AlO partial vapor pressures is over sample **14**, which contains the Ti_2AlC MAX phase. The total vapor pressure over sample **20** of composition 50 mol % Zr_2AlC–50 mol % HfO_2 (Table 1) at low temperatures (1700–1750 K) matches, within the experimental error bar, the total vapor pressure over sample **17** (50 mol % Ti_3AlC_2–50 mol % HfO_2), and at higher temperatures (1790–1820 K), it matches the total vapor pressure over sample **14** (50 mol % Ti_2AlC–50 mol % HfO_2) (Fig. 4). Therefore, the volatility series will be the following: 50 mol % Ti_2AlC–50 mol % HfO_2 < 50 mol % Zr_2AlC–50 mol % HfO_2 < 50 mol %

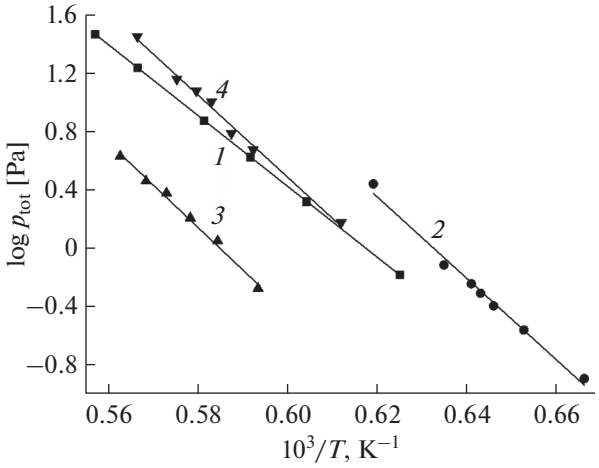

Fig. 3. Total vapor pressure as the sum of Al and Al_2O partial vapor pressures over samples **13**, **16**, **19**, and **22** (Table 1), which contain, mol %: (*1*) $90Ti_2AlC–10HfO_2$, (*2*) $90Ti_3AlC_2–10HfO_2$, (*3*) $90Zr_2AlC–10HfO_2$, and (*4*) $90Zr_3AlC_2–10HfO_2$).

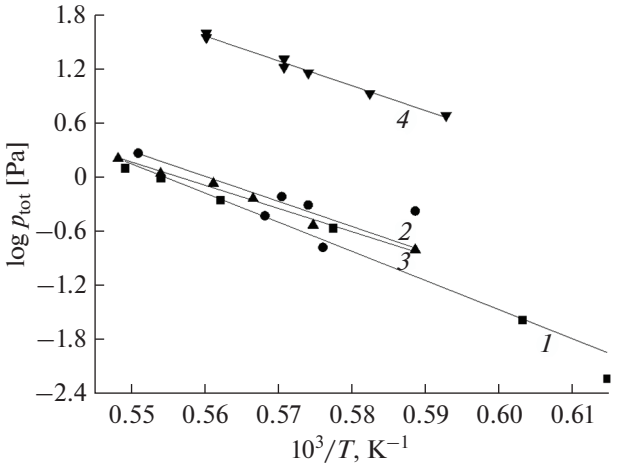

Fig. 4. Total vapor pressure as the sum of Al and Al_2O partial vapor pressures over samples **14**, **17**, **20**, and **23** (Table 1), which contain, mol %: (■, *1*) $50Ti_2AlC–50HfO_2$, (●, *2*) $50Ti_3AlC_2–50HfO_2$, (▲, *3*) $50Zr_2AlC–50HfO_2$, and (▼, *4*) $50Zr_3AlC_2–50HfO_2$.

Ti_3AlC_2–50 mol % HfO_2 ≪ 50 mol % Zr_3AlC_2–50 mol % HfO_2.

In the 80 mol % HfO_2 system, the least sum of the Al and AlO partial vapor pressures is over carbide material **15**, which contains the Ti_2AlC MAX phase. In the temperature range 1720–1850 K, the total vapor pressure over sample **21** (20 mol % Zr_2AlC–80 mol % HfO_2) is comparable (within the experimental error bar) with the total vapor pressure over sample **18** (20 mol % Ti_3AlC_2–80 mol % HfO_2) (Fig. 5). Therefore, the volatility series will be the following: 20 mol % Ti_2AlC–80 mol % HfO_2 < 20 mol % Zr_2AlC–80 mol % HfO_2 ~ 20 mol % Ti_3AlC_2–80 mol % HfO_2 ≪ 20 mol % Zr_3AlC_2–80 mol % HfO_2.

To conclude the work, we compared vaporization processes in samples of aluminum-containing oxycarbide MAX phase systems that have different maximum synthesis temperatures, namely, in Ti_2AlC–HfO_2, Ti_3AlC_2–HfO_2, Zr_2AlC–HfO_2, and Zr_3AlC_2–HfO_2. We should mention here that the results were gathered from samples synthesized at a maximum temperature of 2073 K. In the mass-spectrometric experiment, however, those samples vaporized at lower temperatures (starting 1500–1600 K). Therefore, synthesis at 2073 K might be accompanied with selective vaporization of aluminum from the system and a change in the composition of the condensed phase. To check whether this might indeed occur, we carried out a comparative vaporization of samples synthesized at maximum temperatures of 1773 and 2073 K in systems containing aluminum and 50 mol % HfO_2. It appeared that the vapor composition and partial vapor pressures of Al and Al_2O molecular species over the samples synthesized at 1773 and 2073 K matched each other within the experimental error bar. An exemplary vapor mass spectrum over sample **14** (50 mol % Ti_2AlC–50 mol % HfO_2 according to Table 1) is presented in Table 4. The identical results obtained for samples synthesized at different temperatures indicate the following: a change in the maximum synthesis temperature of samples of the studied oxycarbide systems in the range 1773–2073 K does not change the vapor composition or the partial vapor pressures of molecular species over the sample as determined by Knudsen effusion/mass spectrometry.

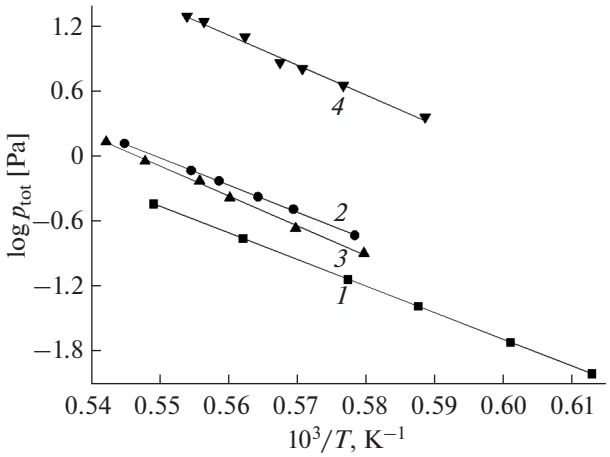

Fig. 5. Total vapor pressure as the sum of Al and Al_2O partial vapor pressures over samples **15**, **18**, **21**, and **24** (Table 1), which contain, mol %: (*1*) $20Ti_2AlC–80HfO_2$, (*2*) $20Ti_3AlC_2–80HfO_2$, (*3*) $20Zr_2AlC–80HfO_2$, and (*4*) $20Zr_3AlC_2–80HfO_2$.

Table 4. Vapor mass spectra over sample **14** (50 mol % Ti_2AlC–50 mol % HfO_2), which was prepared at maximum temperatures of 1773 and 2073 K

T, K	Synthesis temperature, K			
	1773		2073	
	Ion current intensity, arb. units			
	Al^+	Al_2O^+	Al^+	Al_2O^+
1790	23	2.4	24	2.7
1813	38	6.6	37	6.3
1844	52	9.0	52	8.7
1779	21	2.0	22	2.1

CONCLUSIONS

This work is the first where the vaporization of Ti_2SiC, Ti_3SiC_2, Ti_2AlC, Ti_3AlC_2, Zr_2AlC, and Zr_3AlC_2 carbide MAX phase materials and MAX phase–HfO_2 oxycarbide systems was studied up to 2200 K by Knudsen effusion/mass spectrometry. We have shown that carbide materials of as-batch compositions Ti_2SiC and Ti_3SiC_2 are the least volatile and are stable up to 1900 K. Of the studied silicon-containing carbide materials (SiC, Ti_2SiC, and Ti_3SiC_2), the sample of as-batch composition Ti_2SiC has the least total vapor pressure. The vapor over Ti_2SiC and Ti_3SiC_2 samples at temperatures above 1900 K features Si, Si_2, SiC, SiC_2, and Si_2C molecular species, just as over individual silicon carbide. In the vapor over aluminum carbide MAX phase materials, atomic aluminum is the major vapor species at temperatures starting at 1500 K. The relative volatility of the studied aluminum-containing samples has been found to increase in the series $Zr_2AlC < Zr_3AlC_2 < Ti_2AlC < Ti_3AlC_2$.

We have found that hafnia additives to the carbide materials under consideration bring about a decrease in total vapor pressure over the formed oxycarbide systems and give rise to the appearance of oxygen-containing molecular vapor species: SiO and Al_2O, which were not identified in this work over the silicon and aluminum carbide MAX phase materials, respectively. The increasing HfO_2 percentage in aluminum-containing oxycarbide samples changes the order of relative volatilities. When the doping level is 10 mol % HfO_2, samples of Zr_2AlC-containing oxycarbide materials have the least total vapor pressures, as was the case with the above-considered carbide samples. When the HfO_2 percentage increases to 50 mol % or more, however, the system whose composition is formulated as a Ti_2AlC–HfO_2 becomes the least volatile system. Variations in the maximum synthesis temperature in the range 1773–2073 K for samples of the studied oxycarbide systems do not bring about a change in either the qualitative or the quantitative composition of the vapor over the oxycarbide material as determined by Knudsen effusion/mass spectrometry.

SUPPLEMENTARY INFORMATION

The online version contains supplementary material available at https://doi.org/10.1134/S0036023623603045.

ACKNOWLEDGMENTS

The authors are grateful to Dr. Habil. S.N. Perevislov (Grebenshchikov Institute of Silicate Chemistry of the Russian Academy of Sciences) and I.E. Arlashkin (St. Petersburg State Institute of Technology (Technical. University)) for the synthesis of carbide MAX phase materials and samples of oxycarbide systems.

The authors thank the Cryogenic Department of the Science Park at St. Petersburg State University for the uninterrupted supply of liquid nitrogen necessary for the operation of the mass spectrometer.

FUNDING

This work was supported by the federal budget as part of the Government assignment to the Grebenshchikov Institute of Silicate Chemistry of the Russian Academy of Sciences (topic No. 0008-2022-0009, State Register No. 1021050501073-7-1.4.3).

CONFLICT OF INTEREST

The authors declare that they have no conflicts of interest.

REFERENCES

1. M. W. Barsoum, Prog. Solid State Chem. **28**, 201 (2000). https://doi.org/10.1016/S0079-6786(00)00006-6
2. M. Radovic and M. W. Barsoum, Am. Ceram. Soc. Bull. **92**, 20 (2013). https://bulletin-archive.ceramics.org/is-cacheable/1605850406926/ucujko.pdf
3. J. Gonzalez-Julian, J. Am. Ceram. Soc. **104**, 659 (2021). https://doi.org/10.1111/jace.17544
4. D. Y. Kovalev, M. A. Luginina, and S. G. Vadchenko, Russ. J. Inorg. Chem. **62**, 1638 (2017). https://doi.org/10.1134/S0036023617120117
5. E. P. Simonenko, N. P. Simonenko, and I. A. Nagornov, Russ. J. Inorg. Chem. **67**, 705 (2022). https://doi.org/10.1134/S0036023622050187
6. E. P. Simonenko, N. P. Simonenko, I. A. Nagornov, et al., Russ. J. Inorg. Chem. **67**, 1838 (2022). https://doi.org/10.1134/S0036023622601222
7. E. N. Hoffman, D. W. Vinson, R. L. Sindelar, et al., Nucl. Eng. Des. **244**, 17 (2012). https://doi.org/10.1016/j.nucengdes.2011.12.009
8. W. E. Lee, E. Giorgi, R. Harrison, et al., *Ultra-High Temperature Ceramics: Materials for Extreme Environment Ap-*

plications (John Wiley & Sons, Inc., Hoboken, 2014). https://doi.org/10.1002/9781118700853.ch15

9. T. Galvin, N. C. Hyatt, W. M. Rainforth, et al., Nucl. Mater. Energy **22**, 100725 (2020). https://doi.org/10.1016/j.nme.2020.100725
10. V. I. Al'myashev, V. L. Stolyarova, E. V. Krushinov, et a., Tekhnol. Obespech. Zhizn. Tsikla Yadern. Energ. Ustan. **31**, 60 (2023). https://doi.org/10.52069/2414-5726_2023_1_31_60
11. Z. Wen, Z. Tang, H. Meng, et al., Corros. Sci. **207**, 110574 (2022). https://doi.org/10.1016/j.corsci.2022.110574
12. E. K. Kazenas and Yu. V. Tsvetkov, *Evaporation of carbides* (Krasand, Moscow, 2017) [in Russian]. www.rfbr.ru/rffi/portal/books/o_2053121
13. G. H. Rinehart and R. G. Behrens, J. Chem. Thermodyn. **12**, 205 (1980). https://doi.org/10.1016/0021-9614(80)90038-5
14. J. Drowart, G. De Maria, and M. G. Inghram, J. Chem. Phys. **29**, 1015 (1958). https://doi.org/10.1063/1.1744646
15. Z. Cao, W. Xie, I. H. Jung, et al., Metall. Mater. Trans. B: Process Metall. Mater. Process. Sci. **46**, 1782 (2015). https://doi.org/10.1007/s11663-015-0344-8
16. C. A. Stearns and F. J. Kohl, *Mass Spectrometric Determination of the Dissociation Energies of Titanium Dicarbide and Titanium Tetracarbide* (NASA Technical Note D-5653 Cleveland, 1970).
17. Y. L. Li and T. Ishigaki, Mater. Sci. Eng., A **345**, 301 (2003). https://doi.org/10.1016/S0921-5093(02)00506-3
18. C. A. Stearns and F. J. Kohl, *High-Temperature Mass Spectrometry - Vaporization of Group 4-B Metal Carbides* (NASA Technical Note D-7613, Cleveland, 1974). https://ntrs.nasa.gov/search.jsp?R=19740012680 (accessed March 24, 2020)
19. V. J. Keast, S. Harris, and D. K. Smith, Phys. Rev. **80**, 214113 (2009). https://doi.org/10.1103/PhysRevB.80.214113
20. D. Sauceda, P. Singh, A. R. Falkowski, et al., npj Comput. Mater. **7**, 6 (2021). https://doi.org/10.1038/s41524-020-00464-7
21. S. N. Perevislov, T. V. Sokolova, and V. L. Stolyarova, Mater. Chem. Phys. **267**, 124625 (2021). https://doi.org/10.1016/j.matchemphys.2021.124625
22. S. N. Perevislov, V. V. Semenova, and A. S. Lysenkov, Russ. J. Inorg. Chem. **66**, 1100 (2021). https://doi.org/10.1134/S0036023621080210
23. S. N. Perevislov, I. E. Arlashkin, and A. S. Lysenkov, Refract. Ind. Ceram. **63**, 215 (2022). https://doi.org/10.1007/S11148-022-00709-6
24. I. E. Arlashkin and S. N. Perevislov, Materialovedenie **6**, 16 (2023). https://doi.org/10.31044/1684-579X-2023-0-6-16-21
25. I. E. Arlashkin, S. N. Perevislov, and V. L. Stolyarova, Russ. J. Gen. Chem. **93**, 881 (2023). https://doi.org/10.1134/S107036322304014X
26. S. N. Perevislov, I. E. Arlashkin, and V. L. Stolyarova, J. Am. Ceram. Soc. **107,** 488 (2023). https://doi.org/10.1111/jace.19419
27. K. Hilpert, Rapid Commun. Mass Spectrom. **5**, 175 (1991). https://doi.org/10.1002/rcm.1290050408
28. J. Drowart, C. Chatillon, J. Hastie, et al., Pure Appl. Chem. **77**, 683 (2005). https://doi.org/10.1351/pac200577040683
29. S. I. Lopatin, S. M. Shugurov, Z. G. Tyurnina, et al., Glass Phys. Chem. **47**, 38 (2021). https://doi.org/10.1134/S1087659621010077
30. S. I. Lopatin, Glass Phys. Chem. **48**, 117 (2022). https://doi.org/10.1134/S1087659622020055
31. R. C. Paule and J. Mandel, Pure Appl. Chem. **31**, 371 (1972). https://doi.org/10.1351/pac197231030371
32. J. B. Mann, J. Chem. Phys. **46**, 1646 (1967). https://doi.org/10.1063/1.1840917
33. R. T. Meyer and A. W. Lynch, High Temp. Sci. **5**, 192 (1973).
34. S. G. Lias, J. E. Bartmess, J. F. Liebman, et al., J. Phys. Chem. Ref. Data **17**, Suppl. 1, 861 (1988).

Translated by O. Fedorova

SPELL: OK